Biomedical & Pharmacology Journal, March 2025. Vol. **18**(1), p. 701-712

Investigating the Association of Acrylamide with Neurotoxicity: Insights from RNA-Seq and Adverse Outcome Pathways

Ruchi Yadav and Jyoti Prakash*

Amity Institute of Biotechnology, Amity University Uttar Pradesh, Lucknow, UP, India.
Corresponding Author E-mail: jprakash@lko.amity.edu

https://dx.doi.org/10.13005/bpj/3121

(Received: 05 October 2024; accepted: 24 December 2024)

Acrylamide, a neurotoxic compound formed during high-temperature cooking processes, poses significant health risks, particularly regarding neurotoxicity. This study investigates the association between acrylamide exposure and neurotoxic effects, utilizing RNA sequencing (RNA-Seq) to elucidate the underlying molecular mechanisms. Gene expression profiles of neuronal cell models exposed to acrylamide was retrieved from ENA database with project id: PRJNA545942. RNAseq analysis was done to identify significant dysregulation of genes involved in critical cellular processes, including oxidative stress response, apoptosis, and neuroinflammation. Results revealed an upregulation of inflammatory pathway genes and a downregulation of neuroprotective factors, indicating a shift towards a pro-apoptotic and inflammatory state in response to acrylamide exposure. Among the upregulated genes, HMGSC1 and TUBB5 were particularly significant for their association with neurotoxicity pathways. TUBB5 plays a crucial role in neuronal migration and axonal guidance; abnormalities in this gene are severe neurodevelopmental disorders. Findings indicate that acrylamide exposure activates pathways linked to neuronal cell death and impaired neuronal function, providing a clearer understanding of its neurotoxic potential. This research emphasizes RNA-Seq as a valuable tool for investigating acrylamide-induced neurotoxicity and contributes to risk assessment frameworks for chemical exposures. By advancing the understanding of acrylamide's impact on neuronal health, this study lays the groundwork for future studies to mitigate its neurotoxic effects and protect public health.

Keywords: Acrylamide; Adverse Outcome Pathways; Neurotoxicity; RNA-Seq; Variant Analysis.

Acrylamide (ACR) is a type-2 alkene; prolonged exposure to ACR can cause ataxia, weakness in skeletal muscles, developmental defects, reproductive issues, neuronal development, etc[1]. Acrylamide is an aggregate neurotoxin, and reused openness to moderate quantities may cause actual injury to the nervous system. ACR is generally used as a synthetic compound with a neurotoxic effect on warm-blooded animals[2]. Its impact on developmental biology has been studied in several organisms like mammalian models[3]. Acrylamide is a water-soluble alkene primarily used to produce personal care products that include polyacrylamide. It is also utilized in various chemical processes that include the treatment of wastewater, complex cementing processes, and enhancing soil fertility through soil conditioning4. However, exposure to acrylamide, particularly in its monomeric form, has been associated with neurotoxic effects in both humans and animals, leading to symptoms such as muscle weakness, gait abnormalities, and peripheral neurons.[4]

Acrylamide is generally found in plant-based foods, like potatoes, grain products,

brewed coffee, baked foods, ready-to-eat snacks, etc. Studies show that the polymeric form of Acrylamide is non-toxic, while its monomeric form is highly toxic. Researchers have established that exposure to Acrylamide is highly toxic to rodents and mice, exhibiting carcinogenic, teratogenic, and neurotoxic effects[5]. Exposure of Acrylamide to humans causes symptoms of neuronal abnormalities that include symptoms like motor dysfunction, weakness in skeletal muscle, weight loss, ataxia, polyneuropathy, cancer, etc.[6]

Acrylamide-induced neurotoxicity has been associated with central peripheral distal axonopathy[7]. The neurotoxic effects are initiated by acrylamide-forming adducts with sulfhydryl thiolate groups, disrupting essential synaptic vesicle recycling mechanisms. These mechanisms include vesicle docking, involving essential proteins like synaptotagmin, synaptophysin, and syntaxin; vesicle processing mediated by complexin 2; disassembly of the SNARE (soluble N-ethylmaleimide-sensitive factor attachment protein receptor) complex; endocytosis through clathrin; neurotransmitter reuptake via the dopamine transporter; and vesicular storage, regulated by the vesicular monoamine transporter in nerve terminals[8-9].

Researchers have identified the toxicity of acrylamide at the developmental level, and experiments have been widely studied in laboratory animals. However, its specific neurotoxic effects during early development remain underexplored. This gap highlights the need for advanced animal models to examine the impact of acrylamide at the neuronal developmental level and its neurotoxicity. These resources are essential for better clinical supervision of individuals exposed to acrylamide, especially in occupational settings[10]. Zebrafish (Danio rerio) is a standard vertebrate model to study developmental biology and effect of pollutants on it, generally it is used for neurotoxicity research[11]. Its advantages include rapid generation time, high reproductive chances, and a visible body, making it well-suited for toxicity assessments and high-throughput screening of chemical compounds in vivo.

Additionally, the development of the zebrafish brain and central nervous system occurs within just three days post-fertilization, allowing for rapid observation of developmental effects. With approximately 70% DNA sequence homology with humans and comparable neurotransmitter systems, zebrafish are poised to become a fundamental model for bridging the gap between cell-based studies and mammalian testing[12]. Their transparent bodies allow for easy visualization of chemical-induced abnormalities under a stereomicroscope. Although acrylamide-induced acute neurotoxicity has been previously assessed in adult zebrafish using concentrations as high as 0.75 mM (51.31 mg/L), studies on its effects in larval zebrafish are still limited[13].

The zebrafish is a fantastic harmfulness model and biochemical examines can be joined with perceptions at a primary and useful level inside one person valuable level inside one person. This smaller-than-expected audit sums up the power of zebrafish a model for formative neurotoxicity screening, and its prospects to explore working instruments of poisons[14].

Transcriptomic data analysis and annotations

Transcriptome analyses are increasingly conducted using high-throughput RNA sequencing (RNA-seq) techniques. These advanced sequencing methods offer numerous advantages ncluding sequence results at single-base pair resolution, fewer chances of error, and decreased background noise. They also provide a range of expression values that can be detected and analyzed. Additionally, RNA-seq provides higher reproducibility, requires smaller initial RNA sample quantities, and allows for identifying transcripts that may not correspond to a previously sequenced genome[15].

Ongoing specialized and scientific advances make it worthwhile to quantify the articulation of thousands of qualities by equally utilizing cutting-edge sequencing techniques. Significant upgrades in sequencing advances have now given an uncommon freedom to analyze the malignancy genome for enormous scope, distinguishing proof of genomic adjustments in an exhaustive and impartial way[16]. High-throughput mRNA sequencing (RNA-seq) utilizes considerably equal sequencing to permit an unbiased examination of both genome-wide record levels and the transformation status of a tumor. In the RNA-seq strategy, reciprocal DNA (cDNA) produces short succession peruses by immobilizing many intensified DNA parts onto a firm surface and playing out the arrangement response.

The subsequent arrangements are adjusted to a reference genome or record information base to depict the investigated transcriptome[17] accurately.

DESeq2 is a powerful tool for managing RNA-seq data and performing differential gene expression (DEG) analysis. It combines read count data from multiple samples into a comprehensive matrix, with genes organized in rows and samples in columns. DESeq2 applies normalization techniques to account for sequencing depth and library composition variations, ensuring that the resulting counts accurately reflect gene expression levels. Notably, gene length normalization is unnecessary in this analysis, as the focus is on comparing counts of the same gene across different sample groups, allowing for a direct assessment of differential expression.[18]

MATERIAL AND METHODS

RNAseq Data Retrieval

The raw fasta file of paired-end RNA-seq sequencing data for Danio rerio (Zebrafish) was retrieved from NCBI's SRA database. (https://www.ncbi.nlm.nih.gov/sra), (accession ID: PRJNA545942). Brain samples of the control and two ACR-exposed brain samples were downloaded in FASTq format.

Table 1 shows the RNAseq data used for current research. Run IDs SRR9182362 and SRR9182363 were used for ACR-exposed samples, and SRR9182372 and SRR9182373 were used as control samples.

The paired-end sequence for the Brain sample was taken from the ENA database. The. The Instrument model for the sequences was ILLUMINA (Illumina NovaSeq), and the RNA-seq library samples preparation strategy was used in this data; the library layout was Paired seq and organism *Danio rerio.*

RNA-Seq Data analysis

RNA-Seq analysis using Galaxy tools involves a multi-step process to ensure the accurate identification of gene expression patterns and potential genetic variants. The complete workflow and the tools used are shown in Figure 1. The workflow begins with FastQC, which evaluates the quality of raw RNA-Seq reads, followed by Cutadapt[19] to trim adapters and remove low-quality bases, ensuring cleaner reads. Post-trimming

Table 1. List of accession ID, sample name and type of sample Danio rerio. ACR: acrylamide

S. No	Run Accession	Sample FASTQ FTP file link	TYPE
1	SRR9182362	ftp://ftp.sra.ebi.ac.uk/vol1/fastq/SRR918/002/SRR9182362/SRR9182362_1.fastq.gz ftp://ftp.sra.ebi.ac.uk/vol1/fastq/SRR918/002/SRR9182362/SRR9182362_2.fastq.gz	ACR
2	SRR9182363	ftp://ftp.sra.ebi.ac.uk/vol1/fastq/SRR918/003/SRR9182363/SRR9182363_1.fastq.gz ftp://ftp.sra.ebi.ac.uk/vol1/fastq/SRR918/003/SRR9182363/SRR9182363_2.fastq.gz	ACR
3	SRR9182372	ftp://ftp.sra.ebi.ac.uk/vol1/fastq/SRR918/002/SRR9182372/SRR9182372_1.fastq.gz ftp://ftp.sra.ebi.ac.uk/vol1/fastq/SRR918/002/SRR9182372/SRR9182372_2.fastq.gz	CONTROL
4	SRR9182373	ftp://ftp.sra.ebi.ac.uk/vol1/fastq/SRR918/003/SRR9182373/SRR9182373_1.fastq.gz ftp://ftp.sra.ebi.ac.uk/vol1/fastq/SRR918/003/SRR9182373/SRR9182373_2.fastq.gz	CONTROL

quality control is conducted with MultiQC[20], which aggregates and visualizes FastQC reports to confirm improved read quality. Aligned reads are then mapped to the reference genome using RNA STAR[21], generating BAM files for each sample. To assess alignment consistency, MultiBamSummary is used to compute coverage across the genome to assess alignment consistency, offering an overview of alignment quality.

The next step involves quantifying gene expression through featureCounts[22], which counts the aligned reads per gene and generates a count matrix. This matrix is fed into DESeq2 [23] for differential expression analysis, identifying genes with significant changes between conditions. To refine the results, The Filter tool is applied to select differentially expressed genes based on fold change and adjusted p-values to refine the results. These

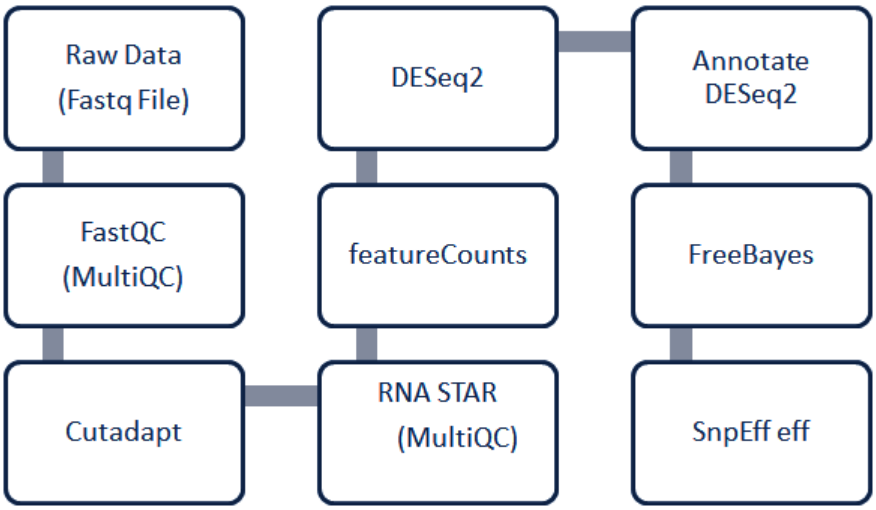

Fig. 1. Work flow for the NGS data analysis to identify differentially expressed genes

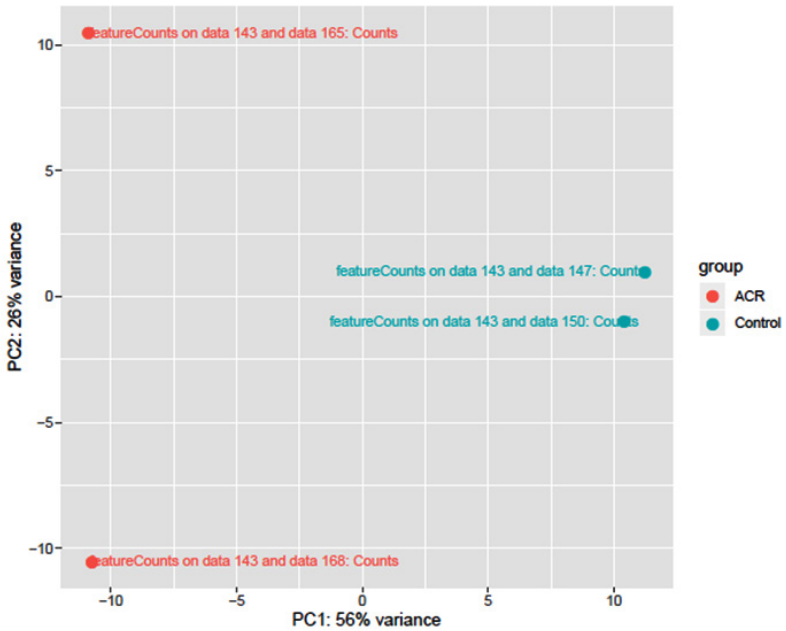

Fig. 2. Scatter plot depicting the first two dimensions obtained from a principal component analysis (PCA) performed on the normalized counts of the samples.

genes are then annotated using Annotate DESeq2[24] to provide functional insights, such as gene names and biological roles. For visualization, Heatmap[25] creates heatmaps to display expression patterns of the top differentially expressed genes across samples for visualization.

Variant calling is carried out using FreeBayes[26], identifying potential SNPs and indels from the RNA-Seq data, with results saved in a VCF file. VCFannotate and SnpEff [27] are used to annotate further and predict the functional effects of the variants, providing a deeper understanding of their impact on gene function. This workflow offers a comprehensive approach to RNA-Seq analysis, utilizing powerful Galaxy tools to study gene expression, regulatory mechanisms, and genetic variants.

Quality Control and Trimming of RNA-Seq Data

To ensure high-quality data for RNA-Seq analysis, initial quality control (QC) checks were performed on the raw FASTQ files using the FastQC tool available on the Galaxy platform. FastQC provides a comprehensive quality assessment by analyzing various metrics, such as base quality scores, GC content, and the presence of adapters. Sequencing errors, including incorrect nucleotide calls and leftover adapter sequences, can introduce biases and misinterpretations of the data. Trimming adapters and low-quality bases is crucial for improving read mapping efficiency. The Cutadapt tool[28] was employed for this, which trims Illumina paired-end and single-end data. The quality control results from FastQC were then aggregated using MultiQC, which provided a combined view of the overall data quality.

Mapping Reads to the Reference Genome

RNA STAR was utilized to align RNA-Seq reads to the reference genome. The trimmed FASTQ files were input into RNA STAR, and paired-end reads were selected for alignment. The Ensembl gene annotation file (GTF) for Danio rerio was imported, and a temporary index of the reference genome was created. The output included a STAR log file, a splice junctions file in BED format, and a BAM file containing the mapped reads. To combine the results of all sample files, STAR log results were used, and the MultiQC tool was performed for further compilation and comparison. The BAM files were visualized using the UCSC Genome Browser and IGV viewer to examine the alignment quality further.

Gene Expression Quantification

The featureCounts tool was used to quantify the number of read sequences mapped and aligned to each gene. The aligned BAM files generated from RNA STAR served as the input. FeatureCounts calculated the number of reads per annotated gene using the reference GTF file. Default parameters were used, and the quality of this count data was assessed using MultiQC, which aggregated the featureCounts summary files for all samples.

Identification of Genes with Differential Expression

Differentially expressed genes (DEGs) prediction and statistical analysis were done using the DESeq2 tool, designed to analyze count data from high-throughput sequencing experiments. The count matrix generated by featureCounts was input into DESeq2, and experimental conditions (e.g., Control vs. ACR) were specified. DESeq2 normalized the data and computed fold changes and p-values for gene expression differences. The data was filtered using the Filter tool to retain genes with an adjusted p-value < 0.05 and an absolute log2 fold change greater than 1. The Annotate DESeq2 tool was used to add additional information, including gene names and genomic coordinates. To visualize these results, the heatmap2 tool was employed, generating heatmaps of the top DEGs. Log2 transformation and data clustering were applied to represent gene expression patterns across conditions better.

Functional Enrichment and Pathway Analysis

Functional enrichment of the differentially expressed genes was done using different databases such as the Gene Ontology (GO) database (https://geneontology.org/), the DAVID database, and the KEGG pathway database, which gives complete annotation of genes. The gene list was uploaded to DAVID, an online tool for functional annotation. GO terms related to biological processes, molecular functions, and cellular components were identified, providing insights into the biological significance of the DEGs. KEGG pathway analysis further revealed key pathways affected by differential gene expression.

Genetic Variant Calling and Annotation

The FreeBayes tool was used to call

variants from the aligned BAM files to identify genetic variants. The reference genome for Danio rerio was selected, and a VCF file containing the identified variants was generated. The SnpEff tool annotated these variants, predicting their potential functional impact. A pre-built SnpEff database for Danio rerio was downloaded and used for variant annotation, providing insights into the effects of these genetic variations.

Homology Modelling and Molecular Docking

Homology modeling was performed using Schrodinger software29, which involved importing the target sequence, identifying model templates, and building the model. Following homology modelling, molecular docking was conducted to predict the gene's structure-function relationship. The docking process included protein and ligand preparation, docking simulations, and visual inspection of binding interactions. These steps provided structural insights into the gene and its potential interactions with ligands.

This comprehensive workflow integrates multiple tools for RNA-Seq data analysis, ensuring high-quality gene expression profiling, variant discovery, and structural prediction.

RESULTS AND DISCUSSION

Comprehensive Analysis and Detection of Differentially Expressed Genes (DEGs)

The DESeq2 tool was employed to identify differentially expressed genes. The input data comprised a count table created through feature counting. The analysis generated three outputs: a normalized count matrix detailing each gene's expression across samples, a graphical representation of all comparisons between samples, and an Annotation file for each gene that includes gene ID, statistical values like log fold change, normalized counts value, p-value, and adjusted p-value.

Figure 2 presents the estimation of variance-mean dependence derived from high-throughput sequencing assays. It specifically features a PCA plot that illustrates the first two dimensions resulting from a principal component analysis performed on the samples' normalized counts. In this visualization, blue dots correspond to the control dataset, whereas red dots denote the ACR dataset.

The MA plot Figure 3 illustrates the logarithm of fold change plotted against the mean

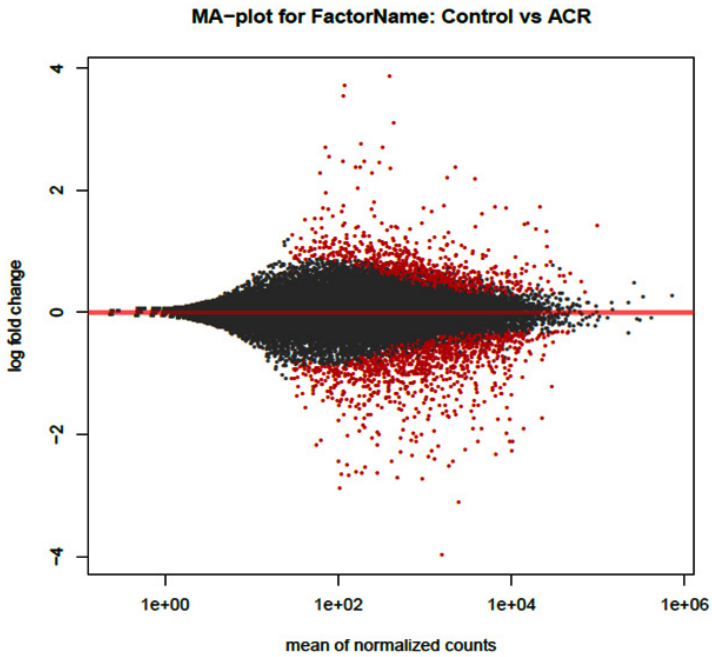

Fig. 3. MA plot for brain samples illustrating the fold change in relation to the mean of normalized counts derived from the DESeq2 dataset.

of the normalized counts. Analysis of the plot reveals that significant gene regulation occurs within the range of -2 to +2. Notably, an important finding is evident for downregulated genes, indicated by red dots in the lower portion of the plot, which exhibit a fold change ranging from -4 to -8. Conversely, the upper half of the plot displays upregulated genes, indicated by red dots, with fold changes ranging from +2 to +6

Figure 4 displays a heatmap plot that illustrates the expression levels of genes across each sample, highlighting the top 20 expressed

Table 2. Top 20 DEGs that are downregulated identified from DESeq2 tool

S.No	GeneID	log2(FC)	P-value	Gene name
1	ENSDARG00000025428	-3.97916	3.34E-71	socs3a
2	ENSDARG00000087303	-3.11943	2.16E-34	cebpd
3	ENSDARG00000106267	-2.88055	7.14E-17	CR388042.1
4	ENSDARG00000058094	-2.723	8.73E-29	ciarta
5	ENSDARG00000037121	-2.70408	3.77E-19	mat2ab
6	ENSDARG00000089429	-2.66139	1.19E-14	si:dkey-205h13.2
7	ENSDARG00000090814	-2.64608	5.27E-15	si:dkey-18a10.3
8	ENSDARG00000053554	-2.63851	1.32E-22	wdr76
9	ENSDARG00000055186	-2.63194	6.72E-16	ccr9a
10	ENSDARG00000001882	-2.61866	3.05E-18	kbtbd12
11	ENSDARG00000091234	-2.53925	1.14E-19	si:ch73-335l21.4
12	ENSDARG00000033160	-2.51107	1.16E-24	nr1d1
13	ENSDARG00000018077	-2.49002	3.66E-13	rbp1.1
14	ENSDARG00000059054	-2.44832	7.71E-22	pdk2b
15	ENSDARG00000043281	-2.44376	1.50E-12	stap2b
16	ENSDARG00000068374	-2.43835	4.48E-23	si:ch211-132b12.7
17	ENSDARG00000056885	-2.41226	9.33E-26	per1a
18	ENSDARG00000002396	-2.36435	5.72E-25	cry-dash
19	ENSDARG00000094210	-2.3461	6.10E-29	fthl31
20	ENSDARG00000010519	-2.32356	4.68E-32	per3

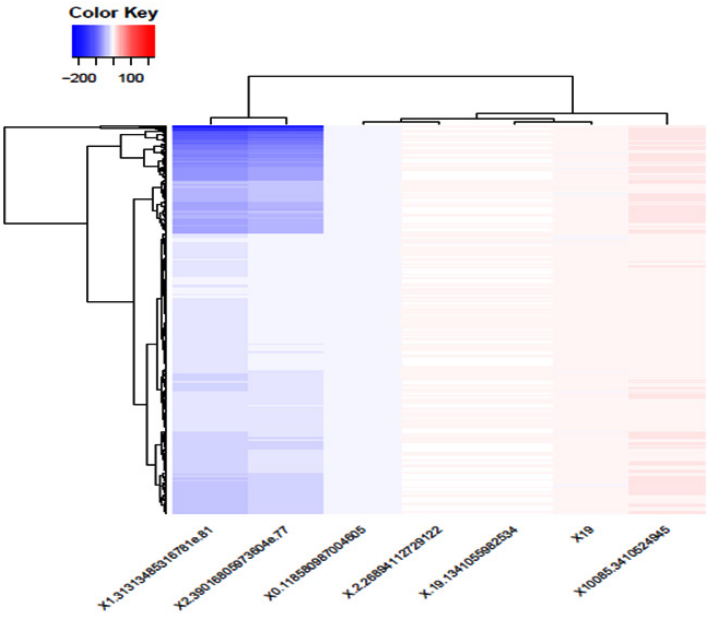

Fig. 4. Heatmap plot of DEG in both samples representing gene ids

genes. Additionally, Table 2 presents the top 10 differentially expressed genes (DEGs), their log fold change (log FC), p-values, and annotations, including Gene ID and Gene name.

In Table 2, a summary for each gene is shown based on a model using the negative binomial distribution. The top 20 differentially expressed genes are shown, which are downregulated. Here, the socs3a gene has a minimum log(FC) value of—3.97916 and a p-value of 3.34E-7.

Table 3 highlights the upregulated genes, among which HMGSC130 and TUBB531 have been linked to neurotoxicity pathways, according to research. The TUBB5 gene is associated with abnormal neuronal migration disorders and impaired axonal guidance. Individuals affected by TUBB5 mutations exhibit microcephaly, ataxia, and severe damage to the development of psychomotor skills. Brain imaging shows that patients suffering from these diseases uncover various malformations in the development cortical region, like white matter and basal ganglia, abnormalities in the development of the corpus callosum, damage in the brainstem and cerebellum region, etc..Functional Profiling and Enrichment of Differentially Expressed Genes

Gene annotation was conducted using the DAVID tool and the Gene Ontology (GO) database. Functional annotation of identified DEGs was identified from the DAVID database (Database for Annotation, Visualization, and Integrated Discovery https://david.ncifcrf.gov). Further, GO

Table 3. Differentially Expressed Upregulated Genes Analyzed Using DESeq2

S.No	GeneID	log2(FC)	P-value	Gene name
1	ENSDARG00000037738	2.039536	4.00E-12	fbxl3l
2	ENSDARG00000017780	2.19036	4.61E-34	rorcb
3	ENSDARG00000103025	2.211373	9.20E-30	hmgcs1
4	ENSDARG00000054202	2.287135	3.66E-11	hbl4
5	ENSDARG00000024488	2.287906	1.54E-15	top2a
6	ENSDARG00000103996	2.366167	9.90E-22	spdl1
7	ENSDARG00000045453	2.370726	7.24E-12	f13a1a.1
8	ENSDARG00000026904	2.383684	2.88E-12	cbln13
9	ENSDARG00000080675	2.386276	5.25E-12	si:dkey-71b5.7
10	ENSDARG00000061274	2.446954	3.09E-23	lss
11	ENSDARG00000039069	2.468816	2.65E-13	slx4ip
12	ENSDARG00000103285	2.474278	3.71E-13	CCDC134
13	ENSDARG00000076573	2.553463	1.57E-13	si:dkey-88j15.3
14	ENSDARG00000015476	2.705268	1.92E-16	iqch
15	ENSDARG00000115830	2.713027	3.62E-15	BX465228.2
16	ENSDARG00000097373	2.759375	1.34E-20	ftr90
17	ENSDARG00000104672	3.109382	6.33E-24	CABZ01074397.1
18	ENSDARG00000095522	3.545447	1.20E-25	si:dkey-71b5.3
19	ENSDARG00000092801	3.71282	2.06E-28	CR855277.2
20	ENSDARG00000087193	3.867054	5.86E-55	prrg2

Table 4. List of differentially expressed genes and their corresponding signaling pathways identified through the Gene Ontology (GO) database

Sr.no	Gene Identifier	Biological Pathway
1	ccr9a	Cytokine- Cytokine receptor interaction
2	Mat2ab	Methionine adenosyl transferase II alpha beta
3	Per3	Herpes simplex infection
4	Hmgsc1	Metabolic pathway
5	Tubb5	Gap junction and phagosome

(Gene Ontology http://geneontology.org) was used to study the biological function of these genes. It provides information on genes in three different categories: MF (Molecular Function), CC (Cellular Component), and BP (Biological Process), which includes detailed information about genes.

Annotation of Biological Pathways

Pathway enrichment analysis was performed to identify the genes associated with tumor- or cancer-related pathways. This analysis was applied to differentially expressed genes, with the most significant genes highlighted in Table 4. The genes identified include ccr9a, mat2ab, per3, hmgsc1, and tubb5. These genes were examined utilizing the Gene Ontology (GO) database to determine their involvement in specific pathways. Table 4 below presents the pathways associated with these differentially expressed genes.

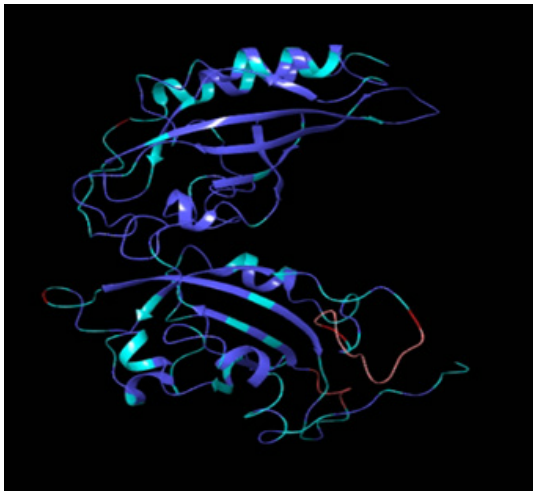

Fig. 5. Homology modeled structure of PER3_ DANRE Uniprot accession number Q9I8L4 .

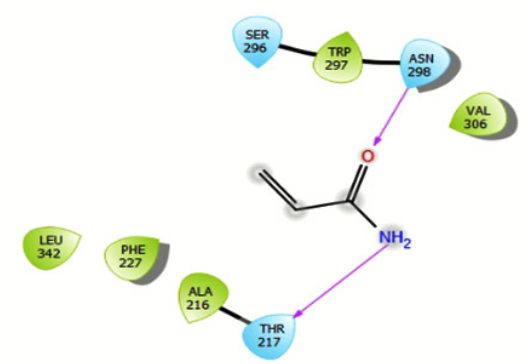

Fig. 6. Acrylamide interaction with per3 protein

The table 4 highlights five genes, each linked to a specific biological pathway, revealing their roles in immune regulation, metabolism, viral response, and cellular communication. *Ccr9a* is involved in immune cell migration within the *Cytokine-Cytokine receptor interaction* pathway, potentially impacting inflammatory diseases. *Mat2ab* plays a key role in methylation processes within cells, essential for gene expression and metabolic balance. *Per3* is associated with immune responses to herpes simplex infection and may influence viral susceptibility based on circadian rhythms. *Hmgsc1* functions in cholesterol biosynthesis within the metabolic pathway, with implications for cardiovascular health. Finally, *Tubb5* supports cellular communication and pathogen clearance, linking it to immune efficiency and neuroprotection. These genes underscore the interconnectedness of critical biological pathways and may inform future therapeutic targets for immune, metabolic, and infectious diseases.

Homology Modeling and Molecular Docking

Homology modelling of the per 3 protein was done using the prime tool of Schrodinger software. The per3 protein sequence was retrieved from the Unipart database with an accession number. Two templates, 4DJ3_A and 4DJ2_A, were used for multi-template homology modelling, with homology scores of 65 and 58%, respectively. Figure 5 shows the modelled structure of the per 2 protein, which was further used for docking.

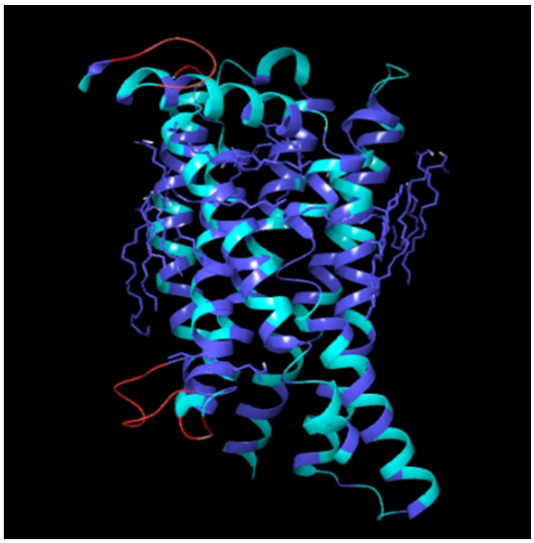

Fig. 7. Homology modeled Structure of ccr9a Uniprot id Q568F5

A glide dock was done between the modeled protein of Per2 and Acrylamide. Figure 6 shows the protein-ligand interaction map, which shows two hydrogen bonds were made at positions Asparagine 298 and Thionine 217 with a glide score of -9 kcal. The docking analysis between the modeled *Per2* protein and acrylamide revealed a strong interaction interaction map shows two hydrogen bonds at Asparagine 298 and Threonine 217, suggesting potential binding sites for acrylamide on *Per2*.

The protein sequence of ccr9a was retrieved from the UniProt database with accession number Q568F5. To predict the structure, two templates were used with PDB id 5LWE_A and 6WWZ_R, respectively, with a 67% and 58% homology score.

Acrylamide's interaction with the ccr9a protein displayed a salt bridge with a glide score of -6 kcal. This salt bridge represents a significant interaction, involving oppositely charged groups in close proximity, which could influence ccr9a protein function. Together, these docking results provide structural insights into how acrylamide binds with Per2 and ccr9a, highlighting possible molecular mechanisms of acrylamide-induced neurotoxicity.

Docking analysis showed that acrylamide forms stable interactions with *Per2* (two hydrogen bonds, glide score -9 kcal) and *ccr9a* (salt bridge, glide score -6 kcal), suggesting these bonds may disrupt normal protein functions and signaling pathways. The study's integrative approach combining bioinformatics and molecular docking highlights potential molecular targets for future neuroprotective interventions and therapeutic strategies against acrylamide-induced toxicity.

CONCLUSION

The development of abnormal cell clusters in the brain can initiate and promote the growth of brain tumors. These irregular cells quickly disrupt brain function and negatively impact the patient's health.This study analyzed RNA sequencing data to identify critical insights, such as which genes show upregulation or downregulation when exposed to acrylamide treatment and their involvement in Gene Ontology (GO) terms or KEGG pathways. To address these questions, this study employed a reference-based RNA-Seq analysis approach on the dataset.

Galaxy provides a practical web-based scientific analysis used to analyse large datasets. The result analysis found sets of down- and up-regulating genes. These genes were then visualized using the UCSC genome browser, showing significant variation to the reference genome. Pathway enrichment analysis was conducted using the DAVID tool and the Gene Ontology (GO) database, and a total of 20 down-regulated and 20 up-regulated genes were found. PER3 and CCR9A genes were down-regulated, and HMGSC1 and TUBB5 were up-regulated. These genes have a significant role in causing neurotoxicity and are involved in the signalling pathways. Further, homology modelling and molecular docking predicted the structure of up-regulated genes using the Schrodinger Maestro tool. An acrylamide reaction was seen in the per3 and ccr9a proteins.

This study highlights neurotoxic pathways and identifying specific up- and down-regulated genes (e.g., PER3, CCR9A, HMGSC1, TUBB5). Additionally, homology modeling and molecular docking provide structural insights into acrylamide's effects on proteins, making this study a valuable foundation for future neurotoxicity research and potential therapeutic development.

Deepening our understanding of acrylamide's effects on neuronal health paves the way for future studies on mitigating its neurotoxic impact and safeguarding public health. This study on acrylamide-induced gene expression changes in the brain has key limitations, including its reliance on reference-based RNA-Seq analysis, which may overlook novel transcripts. Future work should incorporate de novo RNA-Seq to capture novel transcripts, validate findings through in vitro or in vivo experiments. Additionally, exploring the therapeutic potential of key genes (PER3, CCR9A, HMGSC1, TUBB5) and using multi-omics approaches could provide deeper insights into acrylamide's neurotoxic effects and aid in developing preventative strategies.

ACKNOWLEDGEMENT

I would like to acknowledge Amity Institute of biotechnology, Amity University Uttar Pradesh, Lucknow campus for providing us

facilities to conducting this study. This research project is not funded by any specific grant from funding agencies in the public, commercial, or non-profit sectors.

Funding Sources

The author(s) received no financial support for the research, authorship, and/or publication of this article.

Conflict of Interest

The author(s) do not have any conflict of interest.

Data Availability Statement

This statement does not apply to this article.

Ethics Statement

This research did not involve human participants, animal subjects, or any material that requires ethical approval.

Informed Consent Statement

This study did not involve human participants, and therefore, informed consent was not required.

Clinical Trial Registration

This research does not involve any clinical trials

Authors' Contribution

R.Y. (Ruchi Yadav): conceptualization, methodology, data analysis, Visualization, writing; J.P. (Jyoti Prakash): conceptualization, data collection, final approval of the manuscript.

REFERENCES

1. Burwen DR, Banerjee SN, Gaynes RP. Ceftazidime resistance among selected nosocomial gram-negative bacilli in the United States. *J Infect Dis*. 1994;170:1622-5.
2. Friedman M. Chemistry, biochemistry, and safety of acrylamide: a review. *J Agric Food Chem.* 2003;51(16):4504-26.
3. LoPachin RM, Gavin T. Molecular mechanisms of acrylamide neurotoxicity: lessons from organic chemistry. *Environ Health Perspect*. 2012;120(12):1650-7.
4. Tareke E, Rydberg P, Karlsson P, Eriksson S, Törnqvist M. Acrylamide: a cooking carcinogen? *Chem Res Toxicol*. 2000;13(6):517-22.
5. International Agency for Research on Cancer (IARC). Acrylamide. IARC Monogr Eval Carcinog *Risks Hum.* 1994;60:389-433.
6. Shipp A, Lawrence G, Gentry R, McDonald T, Bartow H, Bounds J. Acrylamide: review of toxicity data and dose-response analyses for cancer and noncancer effects. Crit Rev *Toxicol*. 2006;36(6-7):481-608.
7. LoPachin RM. Acrylamide neurotoxicity: neurological, morphological, and molecular endpoints in animal models. *Adv Exp Med Biol*. 2005;561:21-37.
8. Guan H, Zhang Y, He J, Song T, Li W, Sun J. Zebrafish as a model for evaluating the developmental neurotoxicity of acrylamide. *Chemosphere*. 2020;238:124681.
9. Sumner SC, Fennell TR, Moore TA, Chanas B, Gonzalez F, Ghanayem BI. Role of cytochrome P450 2E1 in the metabolism of acrylamide and acrylonitrile in mice. *Chem Res Toxicol*. 1999;12(10):1110-6.
10. National Toxicology Program (NTP). NTP toxicology and carcinogenesis studies of acrylamide. *Natl Toxicol Program Tech Rep Ser*. 2012;575:1-134.
11. Legradi J, el Abdellaoui N, van Pomeren M, Legler J. Comparability of behavioral assays using zebrafish larvae to assess neurotoxicity. *Environ Sci Pollut Res Int*. 2015;22(21):16277-89.
12. Howe K, Clark MD, Torroja CF, Torrance J, Berthelot C, Muffato M. The zebrafish reference genome sequence and its relationship to the human genome. *Nature*. 2013;496(7446):498-503.
13. Hsieh JH, Zhang L, Guyard N, Yan J, Curran K, Xu J. Evaluation of zebrafish embryos as a model for developmental toxicity testing: the International Zebrafish Embryo Screening Consortium's first feasibility study. *Birth Defects Res B Dev Reprod Toxicol.* 2015;104(3):273-91.
14. Holcombe V, Howdeshell KL, Hotchkiss AK, Vorhees CV, Denenberg VH. Neurotoxic effects of acrylamide in adult rats. *Toxicol Sci.* 1995;27(1):124-30.
15. Boverhof DR, Chamberlain MP, Elcombe CR. Comparative metabolism of acrylamide in humans and rodents. *Toxicol Appl Pharmacol*. 2006;214(1):104-10.
16. Wang Z, Gerstein M, Snyder M. RNA-Seq: a revolutionary tool for transcriptomics. *Nat Rev Genet.* 2009;10(1):57-63.
17. Mortazavi A, Williams BA, McCue K, Schaeffer L, Wold B. Mapping and quantifying mammalian transcriptomes by RNA-Seq. *Nat Methods*. 2008;5(7):621-8.
18. Love MI, Huber W, Anders S. Moderated estimation of fold change and dispersion for RNA-seq data with DESeq2. *Genome Biol*. 2014;15(12):550.
19. Martin M. Cutadapt removes adapter sequences

from high-throughput sequencing reads. *EMBnet. journal*. 2011;17(1):10-12.

20. Ewels P, Magnusson M, Lundin S, Käller M. MultiQC: summarize analysis results for multiple tools and samples in a single report. *Bioinformatics*. 2016;32(19):3047-8.
21. Dobin A, Davis CA, Schlesinger F, Drenkow J, Zaleski C, Jha S. STAR: ultrafast universal RNA-seq aligner. *Bioinformatics*. 2013;29(1):15-21.
22. Liao Y, Smyth GK, Shi W. featureCounts: an efficient general-purpose program for assigning sequence reads to genomic features. *Bioinformatics*. 2014;30(7):923-30.
23. Love MI, Huber W, Anders S. Moderated estimation of fold change and dispersion for RNA-seq data with DESeq2. *Genome Biol*. 2014;15(12):550.
24. Warnes GR, Bolker B, Bonebakker L, Gentleman R, Huber W, Liaw A. gplots: various R programming tools for plotting data. *R package version* 2.17.0. 2013.
25. Garrison E, Marth G. Haplotype-based variant detection from short-read sequencing. *arXiv preprint arXiv*:1207.3907. 2012.
26. Cingolani P, Platts A, Wang LL, Coon M, Nguyen T, Wang L. A program for annotating and predicting the effects of single nucleotide polymorphisms, SnpEff. *Fly (Austin)*. 2012;6(2):80-92.
27. Schrödinger, LLC. The Schrödinger Suite 2023-1: Maestro, Desmond, and other modules. New York: Schrödinger, LLC; 2023. Available from: *https://www.schrodinger.com.*
28. Hall B, Gibbons E, Hahm J. Characterization of HMGSC1 as a gene involved in human developmental processes. *Genomics*. 2020;112(5):3782-92.
29. Liu Y, Xie Y, Wang X. TUBB5 overexpression promotes breast cancer progression through the activation of the Wnt/â-catenin signaling pathway. *J Exp Clin Cancer Res*. 2019;38(1):357.
30. Hall B, Gibbons E, Hahm J. Characterization of HMGSC1 as a gene involved in human developmental processes. *Genomics*. 2020;112(5):3782-92.
31. Liu Y, Xie Y, Wang X. TUBB5 overexpression promotes breast cancer progression through the activation of the Wnt/â-catenin signaling pathway. *J Exp Clin Cancer Res*. 2019;38(1):357.